Bifractality of fractal scale-free networks

Jun Yamamoto [1,2,*] and Kousuke Yakubo [1,†]

[1]*Department of Applied Physics, Hokkaido University, Sapporo 060-8628, Japan*
[2]*School of Mathematical Sciences, Queen Mary University of London, London E1 4NS, United Kingdom*

The presence of large-scale real-world networks with various architectures has motivated active research towards a unified understanding of diverse topologies of networks. Such studies have revealed that many networks with scale-free and fractal properties exhibit the structural multifractality, some of which are actually bifractal. Bifractality is a particular case of the multifractal property, where only two local fractal dimensions d_f^{min} and $d_f^{max}(> d_f^{min})$ suffice to explain the structural inhomogeneity of a network. In this work we investigate analytically and numerically the multifractal property of a wide range of fractal scale-free networks (FSFNs) including deterministic hierarchical, stochastic hierarchical, nonhierarchical, and real-world FSFNs. Then we demonstrate how commonly FSFNs exhibit the bifractal property. The results show that all these networks possess the bifractal nature. We conjecture from our findings that any FSFN is bifractal. Furthermore, we find that in the thermodynamic limit the lower local fractal dimension d_f^{min} describes substructures around infinitely high-degree hub nodes and finite-degree nodes at finite distances from these hub nodes, whereas d_f^{max} characterizes local fractality around finite-degree nodes infinitely far from the infinite-degree hub nodes. Since the bifractal nature of FSFNs may strongly influence time-dependent phenomena on FSFNs, our results will be useful for understanding dynamics such as information diffusion and synchronization on FSFNs from a unified perspective.

I. INTRODUCTION

Large-scale networks describing real-world complex systems usually have inhomogeneous structures with large fluctuations in the degree, the number of edges incident to a node. In fact, many complex networks exhibit the scale-free property with power-law degree distributions [1–3]. In order to understand properties of these inhomogeneous networks theoretically, we need to simplify structures of networks. One such simplification is based on an approximation that ignores degree correlations in networks. Owing to the generating function technique, this type of approximation has successfully provided many insights into uncorrelated complex networks [4]. There exist, however, networks whose degree correlations play significant roles. For investigating such strongly correlated networks, it is helpful to focus the fractal nature of a network. A network is fractal with the fractal dimension D_f if the minimum number of subgraphs (boxes) $N_B(l)$ with fixed diameter l required to cover the entire network is proportional to l^{-D_f}. Fractal networks are often contrasted with small-world networks in which $N_B(l)$ decreases exponentially with l. Since the discovery of real-world scale-free networks exhibiting the fractal nature [5], the fractality of complex networks has been extensively studied [6–16]. These studies reveal that many real networks are fractal [10,17–21], at least, on shorter scales than the average

shortest-path distance $\langle l \rangle$ even if the networks exhibit the small-world property on longer scales [12,22].

If a network possesses both the scale-free and fractal properties, a single fractal dimension may not be sufficient to fully describe the fractal nature of the network because the fractal scale-free network (FSFN) could have a multifractal structure [23]. Multifractality is a property of inhomogeneously distributed quantities (probability measures) defined on a fractal object [24]. Although the multifractal nature was initially argued for fractal systems embedded in Euclidean space, it is possible to extend the argument to networks by replacing Euclidean distance with shortest-path distance. In particular, if a measure is evenly assigned to each node, but the distribution of the measure is multifractal, then the network structure itself is considered multifractal. In recent years, numerous studies have presented various efficient algorithms for the multifractal analysis of complex networks and examined the multifractality of many synthetic and real-world networks by utilizing these algorithms [16,25–33]. As an important aspect of FSFNs, it has been shown that a specific class of FSFNs possess *bifractal* structures in which two local fractal dimensions fully characterize the fractal nature of networks [23]. More precisely, an FSFN $\mathcal{G}$ is always bifractal if the number of nodes included in a supernode of the renormalized network of $\mathcal{G}$ is proportional to the degree of the supernode. In fact, FSFNs formed by the (u, v)-flower model [11] and the Song-Havlin-Makse model [6] have been identified as bifractal networks. Since the bifractal property of a network suggests that two qualitatively different behaviors are expected in various local dynamics on the network

---
*j.yamamoto@se22.qmul.ac.uk; jun.j.yamamoto@gmail.com
†yakubo@eng.hokudai.ac.jp

[11,34–36], it is imperative to clarify to what extent FSFNs commonly exhibit bifractal structures. This, however, remains to be revealed. Furthermore, the relationship between the two local fractal dimensions of a bifractal network and the network structure has yet to be elucidated.

In this work we investigate the bifractal property of broader classes of FSFNs. To this end we analyze four types of FSFNs, namely deterministic hierarchical FSFNs formed by the single-generator model [37], stochastic hierarchical FSFNs formed by the multigenerator model, nonhierarchical FSFNs at the percolation critical points, and real-world FSFNs. The combination of these types of networks covers a wide range of FSFNs with a variety of fractal, scale-free, and clustering properties. Our results show that all FSFNs we examined have bifractal structures and we conjecture that any FSFN is bifractal. Furthermore, we study how the bifractality of an FSFN relates to its local fractal structures. In order to identify which part of the network each local fractal dimension d_f describes, we compute d_f around each node in the FSFN by counting the number of nodes $\tilde{v}_i(l)$ within shortest-path distance l from a node i [31]. Our results demonstrate that there exist two distinct substructures with two local fractal dimensions $d_f^{\min}$ and $d_f^{\max}$ in an infinite FSFN. The dimension $d_f^{\min}$ describes the fractality of a region including an infinite-degree hub node, while $d_f^{\max}$ characterizes a region including only finite-degree nodes.

The rest of this paper is organized as follows: Sec. II briefly summarizes the multifractal property of complex networks and the possibility of structural bifractality of FSFNs found by previous studies. Section III shows the bifractal property of various types of FSFNs including deterministic FSFNs formed by the single-generator model, stochastic FSFNs constructed by the multigenerator model, nonhierarchical FSFNs, and real-world FSFNs. In Sec. IV we clarify that each of the two local fractal dimensions of an FSFN characterizes which substructures of the network. We give our conclusions in Sec. V. Hereafter, the terms *distance*, *diameter*, and *radius* are used in the sense of shortest-path distance (chemical distance).

II. MULTIFRACTAL PROPERTY OF NETWORKS

First, we summarize the argument of the multifractal and bifractal properties of complex networks. Consider a simple, connected network $\mathcal{G}$ with the set of nodes $V(\mathcal{G})$ and the set of edges $E(\mathcal{G})$. Let us cover $\mathcal{G}$ with the minimum number of boxes (subgraphs) with a fixed diameter and assume that a probability measure μ_i is defined at each node $i \in V(\mathcal{G})$. The measure μ_i is normalized as $\sum_b \sum_{i \in V(b)} \mu_i = 1$, where $V(b)$ is the set of nodes in a box b of diameter l and the first summation is taken over all the boxes. If the qth moment $Z_q(l)$ of the coarse-grained box measure $\mu_b \equiv \sum_{i \in V(b)} \mu_i$ satisfies

$$Z_q(l) = \sum_b \mu_b^q \propto l^{\tau(q)}, \tag{1}$$

and the mass exponent $\tau(q)$ is nonlinear with respect to q, then we say that the distribution of μ_i is multifractal. Since $\tau(0)$ is identical to $-D_f$, the multifractal distribution of μ_i requires the fractality of $\mathcal{G}$. Moreover, if the relation Eq. (1) stands for a constant measure $\mu_i = \mu_0$ for all $i \in V(G)$, the network structure itself is considered multifractal. In this case

the Hölder exponent $\alpha(q)$ defined by $\alpha(q) = d\tau(q)/dq$ is equivalent to the local fractal dimension d_f describing a substructure in $\mathcal{G}$, because the box measure μ_b is proportional to $l^{\alpha(q)}$, i.e., $\sum_{i \in V(b)} \mu_i \propto l^{\alpha(q)}$, where again l is the box diameter. Due to the nonlinearity of $\tau(q)$, $\alpha(q)$ takes various values depending on q, so a structurally multifractal network is, intuitively, a network in which there exist various substructures described by different values of local fractal dimensions. Previous studies have proposed a number of efficient algorithms for examining the multifractal nature of networks and reported the multifractality of a wide range of synthetic and real-world fractal networks [16,25–33].

If the network $\mathcal{G}$ is not only fractal but also scale-free, $\mathcal{G}$ may possess a *bifractal* structure in which two local fractal dimensions suffice to characterize the fractal nature of $\mathcal{G}$ [23]. In particular, when covering a fractal scale-free network (FSFN) $\mathcal{G}$ with the minimum number of boxes, $\mathcal{G}$ is always bifractal if we have

$$\nu_b \propto k_b, \tag{2}$$

where ν_b is the number of nodes in a box b and k_b is the number of neighboring boxes of b [23]. The quantity k_b is considered to be the degree of the supernode b in the renormalized network of $\mathcal{G}$. As shown in Appendix A, if Eq. (2) holds, the mass exponent $\tau(q)$ is given by

$$\tau(q) = \begin{cases} (q-1)D_f & \text{for } q < \gamma - 1 \\ qD_f\left(\dfrac{\gamma - 2}{\gamma - 1}\right) & \text{for } q \geqslant \gamma - 1 \end{cases}, \tag{3}$$

where γ is the degree exponent describing the asymptotic power-law behavior of the degree distribution $P(k)$, such that $P(k) \propto k^{-\gamma}$ for high degree k. In general, the mass exponent becomes a nonlinear function of q if the measure μ_i varies with site i and is distributed in a multifractal manner. A typical $\tau(q)$ asymptotically approaches $\tau(q) = \alpha_{\max}q$ for $q \to -\infty$, while it approaches $\tau(q) = \alpha_{\min}q$ for $q \to \infty$. The function $\tau(q)$ describing a conventional multifractal system smoothly (nonlinearly) connects these two asymptotic straight lines with different slopes at intermediate q. Thus, the Hölder exponent takes multiple values. We emphasize that the mass exponent given by Eq. (3) has the same form as such a general profile of $\tau(q)$, in which the two asymptotic regions meet each other at $q = \gamma - 1$ and no intermediate region exists. This implies that a bifractal system is a special case of a multifractal system with inhomogeneous local fractality. From Eq. (3), the local fractal dimension equivalent to the Hölder exponent takes two values,

$$d_f^{\max} = D_f,$$
$$d_f^{\min} = D_f\left(\frac{\gamma - 2}{\gamma - 1}\right). \tag{4}$$

Bifractality of FSFNs has been shown [23] analytically for the (u, v)-flower model [11] and numerically for the Song-Havlin-Makse (SHM) model [6]. The theoretical expression of $\tau(q)$ for the (u, v)-flower model has often been used to benchmark newly developed numerical algorithms for multifractal analysis [26,27,30,32,33]. However, the validity of Eqs. (3) and (4) has been verified only for these two kinds of FSFNs, and it remains unclear how common the bifractal
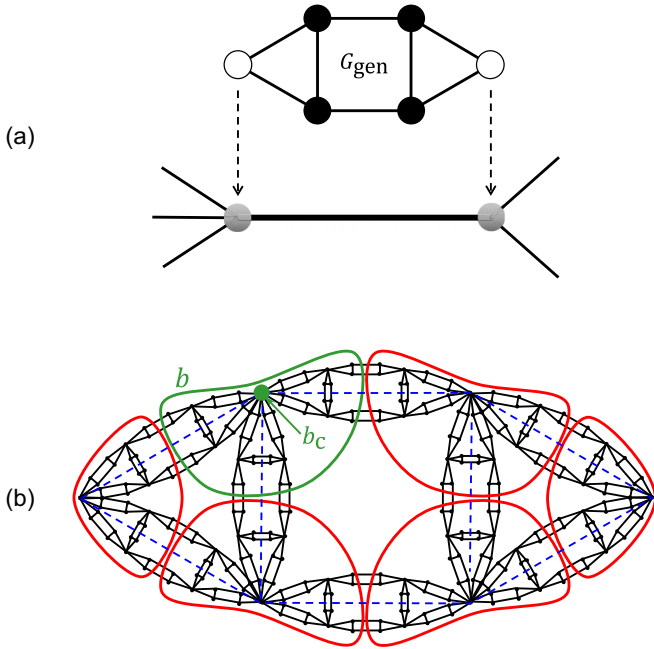
FIG. 1. (a) Example of a generator G_{gen} (top) and the edge replacement by G_{gen}. Two white nodes in G_{gen} represent the root nodes, and four black nodes are the remaining nodes. (b) Box covering [green (left top) and red (other) closed curves] of the third generation network $\mathcal{G}_3$ formed by G_{gen} shown in (a). The six boxes constitute the network $\mathcal{G}_1$ (blue dashed lines). The green, emphasized node is the central node of the green box b. The diameter ($l = 9$) of a box is equal to the diameter of $\mathcal{G}_2$.

property of FSFNs is. In this work we investigate how wide a range of FSFNs satisfies Eq. (2) and exhibits bifractality by examining various conceivable types of FSFNs.

III. BIFRACTALITY OF FSFNs

A. Deterministic hierarchical FSFNs

In order to examine the validity of Eq. (2) [and thus Eqs. (3) and (4)] for a wide range of FSFNs, we first investigate a class of deterministic hierarchical FSFNs formed by the single-generator model [37]. In this model, the tth generation network $\mathcal{G}_t$ is recursively constructed by replacing every edge in $\mathcal{G}_{t-1}$ with a small graph G_{gen} called a generator, so that two root nodes predefined in G_{gen} coincide with the two terminal nodes of the replaced edge, as illustrated by Fig. 1(a). The root nodes of G_{gen} must not be adjacent to each other and have degrees at least two. For simplicity, we concentrate below on the symmetric generator in which a subgraph constructed by removing one root node and its incident edges from G_{gen} has the same topology as a subgraph formed by removing another root node and its incident edges from G_{gen}. It is easy to extend our argument below to the case of an asymmetric generator. We initialize the network $\mathcal{G}_0$ with a single edge with two terminal nodes, so the first generation network $\mathcal{G}_1$ is G_{gen} itself.

Let us consider a generator G_{gen} with m_{gen} edges, in which the two root nodes have degree κ and they are separated by distance λ. The number of nodes in the tth generation network

$\mathcal{G}_t$ by the single-generator model is [37]

$$N_t = 2 + \frac{n_{\text{rem}}(m_{\text{gen}}^t - 1)}{m_{\text{gen}} - 1}, \tag{5}$$

where n_{rem} is the number of "remaining nodes" defined as nodes other than the root nodes in the generator G_{gen}. For $t \gg 1$, $\mathcal{G}_t$ becomes fractal and scale-free. The degree exponent γ and fractal dimension D_{f} are given by

$$\gamma = 1 + \frac{\log m_{\text{gen}}}{\log \kappa}, \tag{6}$$

$$D_{\text{f}} = \frac{\log m_{\text{gen}}}{\log \lambda}. \tag{7}$$

In addition to γ and D_{f}, various properties of $\mathcal{G}_t$, such as the clustering coefficient, degree correlation, and percolation properties, can be analytically obtained by using the quantities determined by the structure of the generator [37]. We can obtain a wide range of deterministic hierarchical FSFNs, including the (u, v)-flower and those by the SHM model, by choosing from a variety of generators.

Here we show that Eq. (2) holds for FSFNs formed by this single-generator model. To this end let us cover the tth generation network $\mathcal{G}_t$ with boxes of fixed diameter l so that the boxes constitute the network $\mathcal{G}_{t'}$ as shown by Fig. 1(b), where $0 \leqslant t' \leqslant t$. Since the boxes in this covering scheme correspond to the *supernodes* of the renormalized network $\mathcal{G}_{t'}$, the number of boxes $N_{\text{B}}(l)$ coincides with the number of nodes in $\mathcal{G}_{t'}$, namely $N_{t'}$ given by Eq. (5). While it is not obvious whether $N_{\text{B}}(l)(= N_{t'})$ provides the minimum number of covering boxes for $\mathcal{G}_t$, $N_{\text{B}}(l)$ would be at least proportional to the minimum number, because we can easily show the relation $N_{\text{B}}(l) \propto l^{-D_{\text{f}}}$ with the fractal dimension D_{f} given by Eq. (7).

In order to count the number of nodes v_b in a box b under this box-covering scheme, we define the central node b_{c} of the box b as the node in $\mathcal{G}_t$ corresponding to the supernode b in $\mathcal{G}_{t'}$. In Fig. 1(b) the green node is the central node of the green box b. The quantity v_b is the number of nodes whose nearest central node is b_{c}. We remark that a superedge [a blue dashed line in Fig. 1(b)] of the renormalized network $\mathcal{G}_{t'}$ represents $\mathcal{G}_{t-t'}$ having $N_{t-t'}$ nodes and half of these nodes are contained in the box b. More precisely, the half of the nodes in $\mathcal{G}_{t-t'}$ other than the two central nodes contribute to v_b from a single superedge. Note that for any node that is equidistant from two central nodes, we consider that half of the node belongs to one box while the other half belongs to another. Such a treatment is justified in the mean-field sense. Denoting the degree of the supernode b as k_b, v_b is given by $k_b(N_{t-t'} - 2)/2 + 1$, where "+1" is the contribution from the central node itself. Therefore, using Eq. (5), we obtain

$$v_b = 1 + k_b \frac{n_{\text{rem}}(m_{\text{gen}}^{t-t'} - 1)}{2(m_{\text{gen}} - 1)}. \tag{8}$$

This relation can be also explained by counting the number of nodes that appear in the growth process from $\mathcal{G}_{t'}$ to $\mathcal{G}_t$, whose nearest node belonging to $\mathcal{G}_{t'}$ is the supernode b. The second term of Eq. (8) dominates the first term for $t \gg t'$, thus we have Eq. (2) for the network $\mathcal{G}_t$ if the box size is much smaller than the size of $\mathcal{G}_t$.
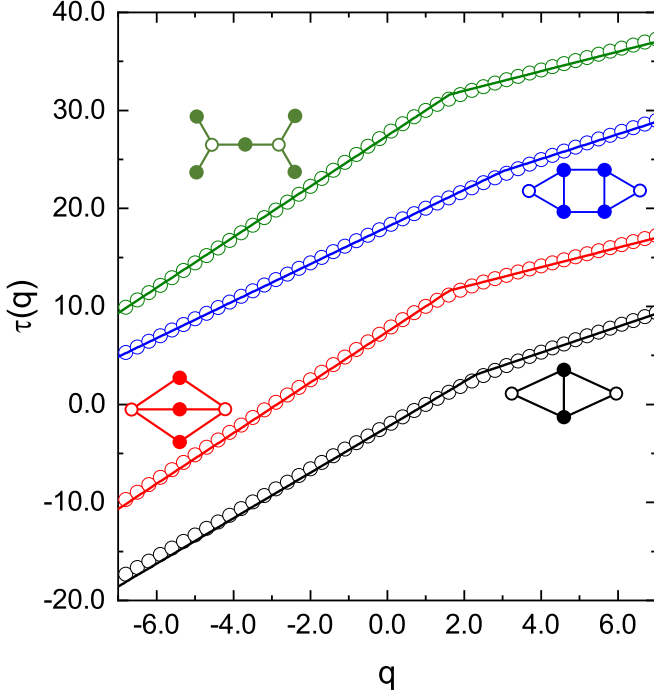
FIG. 2. Mass exponents $\tau(q)$ for deterministic hierarchical FSFNs generated by the single-generator model. Solid lines represent $\tau(q)$'s calculated theoretically by Eq. (9) and symbols indicate those computed numerically by using the sandbox algorithm [27]. Different colors stand for results for different FSFNs. For graphical reasons, the red (second from the bottom), blue (second from the top), and green (top) results are shifted upward by 10, 20, and 30, respectively. The generators employed for our calculations are indicated by small networks in the same colors. Open nodes represent the root nodes. For numerical calculations, the seventh, sixth, fifth, and sixth generation networks formed by the black, red, blue, and green generators are used, which contain 39 064 (78 125), 27 995 (46 656), 18 726 (32 768), and 46 657 (46 656) nodes (edges), respectively.

Since Eq. (2) holds for any $\mathcal{G}_t$ with $t \gg t' \gg 1$, deterministic hierarchical FSFNs formed by the single-generator model exhibit bifractal structures. Using Eqs. (3), (6), and (7), the mass exponent $\tau(q)$ is given by

$$
\tau(q) = \begin{cases} q\dfrac{\log(m_{\text{gen}}/\kappa)}{\log \lambda} & \text{for } q \geqslant \dfrac{\log m_{\text{gen}}}{\log \kappa} \\ (q-1)\dfrac{\log m_{\text{gen}}}{\log \lambda} & \text{for } q < \dfrac{\log m_{\text{gen}}}{\log \kappa} \end{cases}, \quad (9)
$$

and it follows from Eq. (4) that the local fractal dimensions are $d_{\text{f}}^{\max} = \log m_{\text{gen}}/\log \lambda$ and $d_{\text{f}}^{\min} = \log(m_{\text{gen}}/\kappa)/\log \lambda$. To confirm the validity of our theoretical prediction, we have calculated numerically $\tau(q)$ for various FSFNs formed by different generators by applying the sandbox algorithm [27]. As shown in Fig. 2, numerical results agree well with the mass exponent presented by Eq. (9).

B. Stochastic hierarchical FSFNs

While it has been established that numerous hierarchical FSFNs generated by deterministic algorithms display bifractal structures, FSFNs do not necessarily have deterministic

structures. In order to examine the bifractality of stochastic hierarchical FSFNs, we extend the single-generator model to a model with stochastic edge replacements by multiple generators. In this multigenerator model, we prepare a set of s generators $\{G_{\text{gen}}^{(1)}, G_{\text{gen}}^{(2)}, \ldots, G_{\text{gen}}^{(s)}\}$. As in the case of the single-generator model, two nonadjacent root nodes are specified in advance in each generator, where the degrees of the root nodes are 2 or higher. For simplicity, these generators are assumed to be symmetric. To construct the tth generation network $\mathcal{G}_t$, we replace every edge in the previous generation network $\mathcal{G}_{t-1}$ with one of the multiple generators $G_{\text{gen}}^{(i)}$ with the predefined probability $p^{(i)}$, where $\sum_{i=1}^{s} p^{(i)} = 1$. The edge replacement method is the same as that in the single-generator model.

As shown in Appendix B, the number of nodes N_t in the tth generation network $\mathcal{G}_t$ is

$$
N_t = 2 + \frac{\langle n_{\text{rem}} \rangle \big(\langle m_{\text{gen}} \rangle^t - 1\big)}{\langle m_{\text{gen}} \rangle - 1}, \quad (10)
$$

where $\langle m_{\text{gen}} \rangle = \sum_{i=1}^{s} m_{\text{gen}}^{(i)} p^{(i)}$ and $\langle n_{\text{rem}} \rangle = \sum_{i=1}^{s} n_{\text{rem}}^{(i)} p^{(i)}$ are the mean number of edges and the mean number of remaining nodes in a generator averaged over the multiple generators, respectively. Here $m_{\text{gen}}^{(i)}$ and $n_{\text{rem}}^{(i)}$ denote, respectively, the number of edges and the number of remaining nodes in $G_{\text{gen}}^{(i)}$. Appendix B also shows that networks constructed by the multigenerator model exhibit the scale-free and fractal properties as in the case of the single-generator model. The degree exponent γ and fractal dimension D_{f} are given by

$$
\gamma = 1 + \frac{\log\langle m_{\text{gen}} \rangle}{\log\langle \kappa \rangle}, \quad (11)
$$

$$
D_{\text{f}} = \frac{\log\langle m_{\text{gen}} \rangle}{\log\langle \lambda \rangle}, \quad (12)
$$

where $\langle \kappa \rangle = \sum_{i=1}^{s} \kappa^{(i)} p^{(i)}$ is the mean degree of a root node averaged over the multiple generators, and $\kappa^{(i)}$ is the degree of the root node in generator $G_{\text{gen}}^{(i)}$. In addition, $\langle \lambda \rangle$ represents the mean inter-root-node distance. This quantity is determined by the set of distances $\{\lambda^{(i)} : 1 \leqslant i \leqslant s\}$ between the root nodes in the multiple generators, but not the simple average of $\lambda^{(i)}$. Appendix B shows how $\langle \lambda \rangle$ is calculated from $\{\lambda^{(i)}\}$. It should be emphasized that the multigenerator model encompasses a much broader class of FSFNs than that of the single-generator model because $\langle m_{\text{gen}} \rangle$, $\langle \kappa \rangle$, and $\langle \lambda \rangle$ can take noninteger values.

We cover the network $\mathcal{G}_t$ with boxes of a fixed diameter as we did for the single-generator model. Namely, $\mathcal{G}_t$ is covered so that the covering boxes constitute the network $\mathcal{G}_{t'}$ with $t' \ll t$, where $\mathcal{G}_{t'}$ is a network appearing in the stochastic construction process from $\mathcal{G}_0$ to $\mathcal{G}_t$. A box b contains half of the nodes within the subgraphs constituting k_b superedges from the supernode b in the renormalized network $\mathcal{G}_{t'}$, as in the single-generator model, but these superedges stand for different realizations of $\mathcal{G}_{t-t'}$ in this stochastic model. However, if $t \gg t' \gg 1$, i.e., the superdegree k_b and sizes of networks $\mathcal{G}_{t-t'}$ are large enough, then we can approximate the number of nodes ν_b in the box b as $\nu_b = k_b(N_{t-t'} - 2)/2 + 1$, where $N_{t-t'}$ is given by Eq. (10). This leads to Eq. (8) for ν_b with n_{rem} and m_{gen} replaced by $\langle n_{\text{rem}} \rangle$ and $\langle m_{\text{gen}} \rangle$, respectively. Since Eq. (2) holds when $N_{t-t'} \gg 1$ for $t \gg t'$, we can conclude that stochastic hierarchical FSFNs formed by the multigenerator
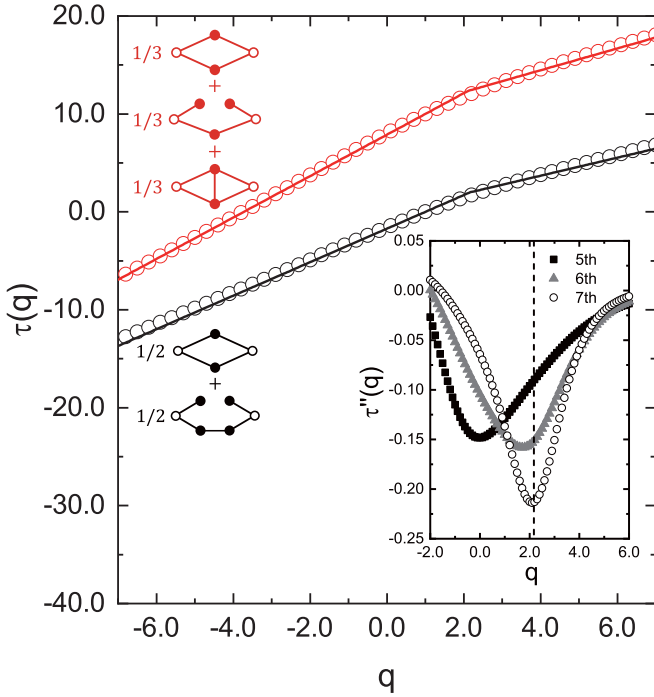
FIG. 3. Mass exponents $\tau(q)$ for stochastic hierarchical FSFNs generated by the multigenerator model. Solid lines represent $\tau(q)$'s calculated theoretically by Eq. (13), and symbols indicate those computed numerically for seventh generation networks averaged over 100 [black (bottom) results] or 50 [red (top) results] realizations by using the sandbox algorithm [27]. Different colors stand for results for different combinations of generators indicated by small networks in the same colors. Fractions beside the generators represent the edge replacement probabilities. For graphical reasons, the red results are shifted upward by 10. The inset shows the numerically calculated second derivatives of $\tau(q)$ for fifth, sixth, and seventh generation FSFNs formed by the combination of black generators. The vertical dashed line indicates the folding point of $\tau(q)$ that is theoretically predicted.

model possess bifractal structures. Using Eqs. (3), (11), and (12), the mass exponent $\tau(q)$ is given by

$$\tau(q) = \begin{cases} q\dfrac{\log(\langle m_{\text{gen}}\rangle/\langle\kappa\rangle)}{\log\langle\lambda\rangle} & \text{for } q \geqslant \dfrac{\log\langle m_{\text{gen}}\rangle}{\log\langle\kappa\rangle} \\ (q-1)\dfrac{\log\langle m_{\text{gen}}\rangle}{\log\langle\lambda\rangle} & \text{for } q < \dfrac{\log\langle m_{\text{gen}}\rangle}{\log\langle\kappa\rangle} \end{cases}, \quad (13)$$

and it follows from Eq. (4) that the two local fractal dimensions are $d_{\text{f}}^{\max} = \log\langle m_{\text{gen}}\rangle/\log\langle\lambda\rangle$ and $d_{\text{f}}^{\min} = \log(\langle m_{\text{gen}}\rangle/\langle\kappa\rangle)/\log\langle\lambda\rangle$. The above theoretical prediction has been confirmed numerically by computing $\tau(q)$ for FSFNs formed by the multigenerator model with two and three generators. Our results are shown in Fig. 3. Although the numerical results for seventh generation networks deviate slightly from $\tau(q)$ presented by Eq. (13), they are basically in agreement with the theoretical results. Such deviations are caused by finite-size effects. As expected from our analytical argument, Eq. (2) holds in the multigenerator model when $t \gg t' \gg 1$ and the bifractal behavior of $\tau(q)$ is realized in large FSFNs. The sizes of FSFNs employed for numerical calculations (on

average, $N_7 = 32\,030$ and $20\,085$ for black and red results in Fig. 3, respectively) may not be large enough. To investigate the finite-size effect, we calculate the q dependence of the second derivative $\tau''(q)$, namely, the curvature of $\tau(q)$. The results shown in the inset of Fig. 3 demonstrate that as the generation of FSFNs increases, $\tau(q)$ begins to fold abruptly and the folding point approaches the theoretical value $q = \log\langle m_{\text{gen}}\rangle/\log\langle\kappa\rangle$. While Fig. 3 shows $\tau''(q)$ only for the combination of black generators, we obtained similar results also for the red generator combination. Furthermore, Eq. (13) has been confirmed for various combinations of generators other than those shown in Fig. 3.

C. Nonhierarchical FSFNs

Structures of networks treated so far are, by construction, hierarchical. Do FSFNs with less clear hierarchical structures also exhibit the bifractal property? To answer this question, we investigate giant connected components of uncorrelated scale-free networks at their percolation critical points. If the degree distribution of a scale-free random network (SFRN) $\mathcal{G}$ at criticality is given by $P(k) \propto k^{-\gamma}$ for high degree k, then the degree distribution $P_{\text{GC}}(k)$ of the giant component $\mathcal{G}_{\text{GC}}$ of $\mathcal{G}$ follows $P_{\text{GC}}(k) \propto k^{-\gamma'}$ with $\gamma' = \gamma - 1$ [38]. In addition, $\mathcal{G}_{\text{GC}}$ takes a fractal structure with the fractal dimension $D_{\text{f}} = 2$ for $\gamma \geqslant 4$ or $D_{\text{f}} = (\gamma - 2)/(\gamma - 3)$ for $3 < \gamma < 4$ [39]. These facts imply that $\mathcal{G}_{\text{GC}}$ is an FSFN.

Let us cover the giant component $\mathcal{G}_{\text{GC}}$ with boxes, each of which consists of nodes within distance l from a central node of degree k, and count the number of nodes ν_b in a box b. We should note here that $\mathcal{G}_{\text{GC}}$ exhibits a long-range degree correlation though $\mathcal{G}$ is uncorrelated. In general, long-range degree correlations of networks are described by the conditional probability $P(k, k'|l)$ of randomly chosen two nodes separated by l from each other having degrees k and k' or the probability $P(k'|k, l)$ that a node separated by l from a randomly chosen node of degree k has degree k' [40]. These probabilities for the giant component of a random network, $P_{\text{GC}}(k, k'|l)$ and $P_{\text{GC}}(k'|k, l)$, have been studied by Mizutaka and Hasegawa [41] for the case that the third moment $\sum_k k^3 P(k)$ is finite. In particular, the probability $P_{\text{GC}}(k'|k, l)$ is given by

$$P_{\text{GC}}(k'|k, l) = \frac{1 - v^{l-1}u^{k+k'-2}}{1 - v^{l-1}u^k}\frac{k'P(k')}{z_1}, \quad (14)$$

where u is the solution of $u = G_1(u)$ with the generating function $G_1(u)$ defined by $G_1(u) = \sum_k kP(k)u^{k-1}/z_1$, $v = G_1'(u)/G_1'(1)$, and $z_1 = \sum_k kP(k)$. Since u is the probability that an edge does not lead to the giant component, we have $u < 1$ in the percolating phase and $u = 1$ at the critical point. Assuming that $u = 1 - \varepsilon$ with a small positive quantity ε near the critical point, we have $v = 1 - (z_3/z_2)\varepsilon$, where $z_2 = \sum_k k(k-1)P(k)$ and $z_3 = \sum_k k(k-1)(k-2)P(k)$. Substituting these expressions of u and v into Eq. (14) and taking the limit of $\varepsilon \to 0$, $P_{\text{GC}}(k'|k, l)$ at criticality is given by

$$P_{\text{GC}}(k'|k, l) = \frac{z_3(l-1) + z_2(k+k'-2)}{z_3(l-1) + z_2 k}\frac{k'P(k')}{z_1}, \quad (15)$$

if z_3 is finite. We utilize this probability to examine analytically the validity of Eq. (2) for $\mathcal{G}_{\text{GC}}$ at criticality under the condition of finite z_3 (i.e., $\gamma > 4$).

In order to calculate the number of nodes ν_b in the box b, we first consider the number of nodes of degree k' at distance l from a node i_k of degree k. Denote this quantity by $n(k'|k, l)$. Assuming that $\mathcal{G}_{GC}$ at the critical point has a tree structure, $n(k'|k, l)$ satisfies the following relation:

$$n(k'|k, l) = P_{GC}(k'|k, l) \sum_{k''} (k'' - 1) n(k''|k, l - 1). \quad (16)$$

In this recurrence relation, the sum in the right-hand side represents the number of nodes at distance l from the node i_k. The quantity $n(k'|k, l)$ at $l = 1$ is obviously given by $n(k'|k, l = 1) = kP_{GC}(k'|k, l = 1)$. Thus, using Eq. (15), we have

$$n(k'|k, l = 1) = \frac{1}{z_1}(k + k' - 2)k'P(k'). \quad (17)$$

Under this initial condition, the solution of the recurrence equation Eq. (16) reads

$$n(k'|k, l) = \frac{1}{z_1^2} \big[(l - 1)z_3 + (k + k' - 2)z_1 \big] k'P(k'). \quad (18)$$

Here we used the equality $z_1 = z_2$ at the critical point [42]. Since the number of nodes $n_l(k)$ at distance l from the node i_k of degree k is given by $n_l(k) = \sum_{k'} n(k'|k, l)$, it follows from Eq. (18) that

$$n_l(k) = \frac{1}{z_1}[(l - 1)z_3 + kz_1]. \quad (19)$$

Therefore, the number of nodes $\nu_{b(l)}$ in the box $b(l)$ consisting of nodes within distance l from the central node i_k of degree k, given by $\nu_{b(l)} = 1 + \sum_{l'=1}^{l} n_{l'}(k)$, is expressed as

$$\nu_{b(l)} = 1 + \frac{z_3}{2z_1}l(l - 1) + kl. \quad (20)$$

On the other hand, the number of neighboring boxes $k_{b(l)}$ of $b(l)$ is equivalent to $n_{l+1}(k)$ under the tree approximation for $\mathcal{G}_{GC}$, because each of the nodes at distance $l + 1$ from node i_k belongs to a separate neighboring box. Hence, Eq. (19) gives

$$k_{b(l)} = \frac{z_3}{z_1}l + k. \quad (21)$$

When we cover a huge scale-free $\mathcal{G}_{GC}$ with the minimum number of boxes, the degree k of the central node of a box becomes quite large, and we can approximate Eqs. (20) and (21) as $\nu_{b(l)} \simeq kl$ and $k_{b(l)} \simeq k$. Therefore, Eq. (2) holds also for the giant component $\mathcal{G}_{GC}$ of an SFRN at the percolation critical point, and we can conclude that $\mathcal{G}_{GC}$, an example of nonhierarchical FSFNs, shows the bifractal property.

The above analytical argument is valid only for $\gamma > 4$, but there is no obvious reason that $\mathcal{G}_{GC}$ is not bifractal for $\gamma \leqslant 4$. Thus, it is plausible that the giant component in a critical SFRN is bifractal independently of γ. If this is the case, considering that $P_{GC}(k) \propto k^{-\gamma'}$ with $\gamma' = \gamma - 1$ and $D_f = 2$ for $\gamma \geqslant 4$ or $D_f = (\gamma - 2)/(\gamma - 3)$ for $3 < \gamma < 4$, the mass exponent $\tau(q)$ for $\mathcal{G}_{GC}$ is given by

$$\tau(q) = \begin{cases} q & \text{for } q \geqslant \gamma - 2 \\ (q - 1)\dfrac{\gamma - 2}{\gamma - 3} & \text{for } q < \gamma - 2 \end{cases}, \quad (22)$$

for $3 < \gamma < 4$, or

$$\tau(q) = \begin{cases} 2q\left(\dfrac{\gamma - 3}{\gamma - 2}\right) & \text{for } q \geqslant \gamma - 2, \\ 2(q - 1) & \text{for } q < \gamma - 2 \end{cases} \quad (23)$$

for $\gamma \geqslant 4$. The local fractal dimensions are then $d_f^{\max} = (\gamma - 2)/(\gamma - 3)$ and $d_f^{\min} = 1$ for $3 < \gamma < 4$ or $d_f^{\max} = 2$ and $d_f^{\min} = 2(\gamma - 3)/(\gamma - 2)$ for $\gamma \geqslant 4$.

To confirm the above arguments numerically, we prepare SFRNs formed by the configuration model [4,43]. The degree distribution is chosen as

$$P(k) = \frac{c}{k^\gamma + d^\gamma}, \quad (24)$$

for $1 \leqslant k \leqslant 1000$ and $P(0) = P(k > 1000) = 0$, which is proportional to $k^{-\gamma}$ for $k \gg d$. The parameter d can control the moments of $P(k)$ and c is the normalization constant. The value of d for a given γ is chosen so that the critical condition $\langle k^2 \rangle / \langle k \rangle = 2$ [42] is satisfied. We employed two values of γ, i.e., $\gamma = 4.25$ and 3.75. The parameter d for these values of γ takes $d = 1.534$ (for $\gamma = 4.25$) and 1.075 (for $\gamma = 3.75$). The giant components in these networks are fractal with the fractal dimensions $D_f = 2$ (for $\gamma = 4.25$) and 2.33 (for $\gamma = 3.75$). As shown in Fig. 4, the mass exponents $\tau(q)$ for the giant components in these SFRNs support the theoretical prediction for both $\gamma > 4$ and $\gamma \leqslant 4$. As in the case of stochastic hierarchical FSFNs, the inset in Fig. 4 shows that the deviation from the theoretical prediction due to the finite-size effect decreases as the system size increases.

D. Real-world FSFNs

Our arguments so far demonstrate that many types of FSFNs possess bifractal structures, which leads us to suspect that any FSFN is bifractal. This is plausible also from the following considerations. Assume that $\mathcal{G}$ is an FSFN. When $\mathcal{G}$ is covered by boxes of diameter l, these boxes and connections between them construct a renormalized network $\mathcal{G}'$. As in the case of deterministic hierarchical FSFNs, we can define the central node b_c of a box b as the node in $\mathcal{G}$ corresponding to the supernode b in $\mathcal{G}'$. Due to the fractal nature of $\mathcal{G}$, the renormalized network $\mathcal{G}'$ can be regarded as a network with these central nodes and equivalent (in a statistical sense) superedges connecting central nodes [see Fig. 1(b)]. Thus, the original subgraphs in $\mathcal{G}$ corresponding to these superedges have almost the same number of nodes n. If the degree of the supernode b is k_b in $\mathcal{G}'$, k_b superedges are connected to the central node b_c. The number of nodes ν_b in the box b is then given by $\nu_b \simeq nk_b/2$, which realizes Eq. (2). Therefore, we can expect that any kind of FSFN exhibits a bifractal structure.

To check the above conjecture, two kinds of real-world FSFNs have been numerically analyzed. One is the World Wide Web (WWW) of the University of Notre Dame [44] with 325 729 nodes, and the other is the largest connected component of the human protein interaction network (PIN) [45] with 2217 nodes. Data for both networks are freely available at the "Netzschleuder Network Catalog and Repository" [46]. Treating the WWW as undirected, we computed the degree distributions $P(k)$ for these networks and observed the power-law behaviors of $P(k)$ with the exponents $\gamma = 2.75 \pm 0.08$ and 2.59 ± 0.22 for the WWW and PIN, respectively. To
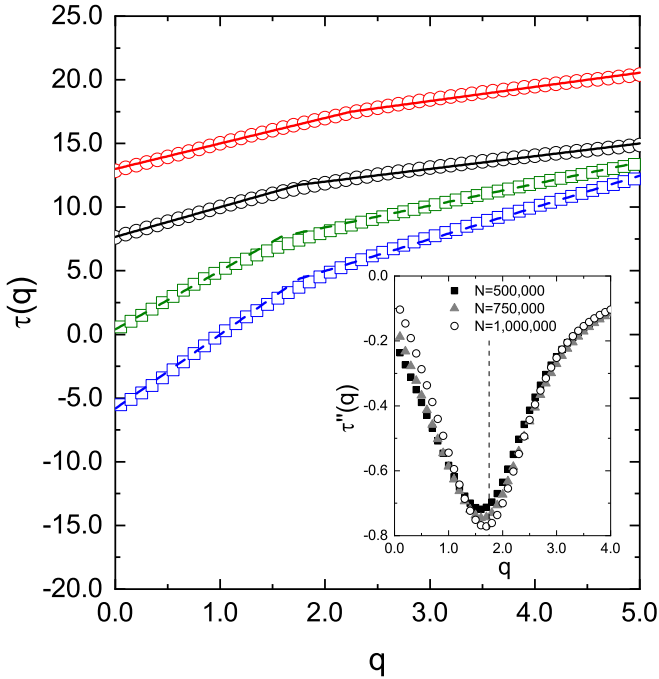
FIG. 4. Mass exponents $\tau(q)$ for nonhierarchical FSFNs (open circles and solid lines) and for real-world FSFNs (open squares and dashed lines). Solid lines represent $\tau(q)$'s calculated theoretically for the giant components in SFRNs at the percolation critical point, which are given by Eq. (22) or (23). Open circles indicate those computed numerically by using the sandbox algorithm [27] for the giant components in critical SFRNs ($N = 10^6$) formed by the configuration model. Black (second from the top) and red (top) data show results for the degree exponents $\gamma = 3.75$ and 4.25, respectively. Numerical results are averaged over 100 realizations and the average giant component sizes are 12 829.8 for $\gamma = 3.75$ and 14 631.4 for $\gamma = 4.25$. The inset shows the numerically calculated second derivatives of $\tau(q)$ for the giant components in critical SFRNs with 5.0×10^5, 7.5×10^5, and 10^6 nodes and for $\gamma = 3.75$. The vertical dashed line indicates the folding point of $\tau(q)$ that is theoretically predicted. Blue (bottom) and green (second from the bottom) squares in the main panel indicate the mass exponents $\tau(q)$ for the World Wide Web and protein interaction network calculated by the sandbox algorithm. Colored dashed lines represent $\tau(q)$ given by Eq. (3) with γ and D_f measured for these real-world networks. For graphical reasons, the red, blue, and green results are shifted upward by 10, 20, and 30, respectively.

ensure consistency with the multifractal analysis, we measured the fractal dimensions of these networks using the sandbox method, and found $D_f = 5.82 \pm 0.10$ for the WWW and 4.60 ± 0.60 for the PIN. As shown in Fig. 4, the mass exponents predicted by Eq. (3) with these observed values of γ and D_f well reproduce $\tau(q)$ calculated numerically for these real networks. These results support our conjecture that any FSFN including real-world networks is bifractal.

IV. LOCAL FRACTAL DIMENSION

The bifractal property of an FSFN implies that there exist two local fractal dimensions in the network. It is, however, unclear which substructures of the network are characterized

by $d_f^{\min}$ and $d_f^{\max}$. To clarify the correspondence between the substructures and the two local fractal dimensions, we examine the local structure centered around each node i in a tth generation network $\mathcal{G}_t$ formed by the single-generator model argued in Sec. III A. Let node i be one of the nodes that first appears in the t_0-th generation ($1 \leqslant t_0 \ll t$), and k be the initial degree of this node when it first appears. Then the degree k_t of the node i in $\mathcal{G}_t$ is given by

$$k_t = k\kappa^{t-t_0}, \quad (25)$$

where κ is the degree of the root node in the generator G_{gen}. Since we assume $t \gg t_0$, the node i is a hub node with high degree k_t. Now, we count the number of nodes $\tilde{v}_{t'}$ in $\mathcal{G}_t$ within distance $L_{t'}$ from the node i, where $L_{t'}$ is the diameter of the t'th generation network $\mathcal{G}_{t'}$ with $1 \ll t' \leqslant t - t_0$. Since there exist $k\kappa^{t-t_0-t'}$ subgraphs $\mathcal{G}_{t'}$ within distance $L_{t'}$ from the node i, we have

$$\tilde{v}_{t'} = (N_{t'} - 1)k\kappa^{t-t_0-t'} + 1$$
$$\simeq N_{t'}k\kappa^{t-t_0-t'}, \quad (26)$$

where $N_{t'}$ is the number of nodes in $\mathcal{G}_{t'}$. Equation (5) for $N_{t'}$ with $t' \gg 1$ gives

$$N_{t'} \simeq m_{\text{gen}}N_{t'-1}. \quad (27)$$

Thus, it follows from Eqs. (26) and (27) that

$$\tilde{v}_{t'} = \left(\frac{m_{\text{gen}}}{\kappa}\right)\tilde{v}_{t'-1}. \quad (28)$$

On the other hand, since each edge on the longest path in $\mathcal{G}_{t'-1}$, which determines its diameter $L_{t'-1}$, is replaced in $\mathcal{G}_{t'}$ with the generator G_{gen} whose root nodes are separated by λ from each other, the diameter $L_{t'}$ of $\mathcal{G}_{t'}$ is given by

$$L_{t'} = \lambda L_{t'-1}. \quad (29)$$

Equations (28) and (29) indicate that when the radius $L_{t'-1}$ is multiplied by λ, the number of nodes $\tilde{v}_{t'-1}$ is multiplied by m_{gen}/κ. This implies that the local fractal dimension around the node i is $\log(m_{\text{gen}}/\kappa)/\log \lambda$, which is equal to $d_f^{\min}$ of a network formed by the single-generator model. This argument holds even if we take the limit of $t \to \infty$ while keeping t_0 finite. In this limit k_t in Eq. (25) diverges. Therefore, in the thermodynamic limit where bifractality in the strict sense is established, fractality around a hub node with an infinitely high degree is described by the local fractal dimension $d_f^{\min}$.

Even in the thermodynamic limit, the fraction of infinite-degree hub nodes is infinitesimal, and almost all of the nodes have finite degrees [11]. A substructure around a finite-degree node located at finite distance l_0 from an infinite-degree hub node will have the same fractality as that around the infinite-degree hub node at the scale of $l \gg l_0$. Thus, the local fractal dimension around such a finite-degree node is also $d_f^{\min}$. The fraction of these finite-degree nodes near hubs is, however, still zero, and the overwhelming majority are the remaining finite-degree nodes that are infinitely far from infinite-degree hub nodes. This can be also understood from the behavior of the singularity spectrum $f(\alpha)$, which is the Legendre transform of $\tau(q)$. Performing the Legendre transformation on $\tau(q)$ given by Eq. (3), we have $f(\alpha_{\min}) = 0$ and $f(\alpha_{\max}) = D_f$. This implies that the hub nodes corresponding to $\alpha_{\min}(= d_f^{\min})$
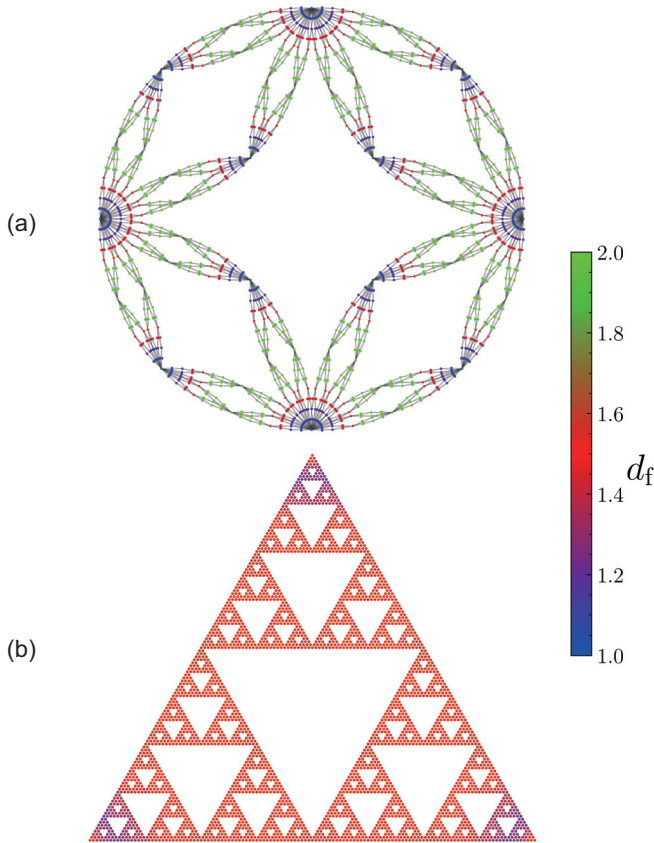
FIG. 5. Distribution of the local fractal dimension d_f on (a) the sixth generation (2,2)-flower and (b) seventh generation Sierpinski gasket. Colors on nodes indicate values of d_f.

have a pointlike measure, while the nonhub regions corresponding to $\alpha_{max}(= d_f^{max})$ are extended with the same fractal dimension as D_f for the entire network. The argument on the fractality around hub nodes cannot be applied to the substructure around such a finite-degree node i. This is because $t - t_0$ must be finite for the degree k_t of the node i to be finite, and Eq. (26) requiring the condition $t' \leqslant t - t_0$ is valid only in a narrow range of $L_{t'}$. Considering that finite-degree nodes infinitely far from infinite-degree nodes dominate the whole network, the local fractality around such a finite-degree node must be described by the global fractal dimension D_f which is identical to d_f^{max}. Therefore, the lower local fractal dimension d_f^{min} reflects the fractality of substructures around infinitely high degree hub nodes and finite-degree nodes at finite distances from these hub nodes, while the higher local fractal dimension d_f^{max} characterizes the local fractality around finite-degree nodes infinitely far from infinite-degree hub nodes. We numerically investigate the local fractal dimension for the sixth generation (2,2)-flower ($N_6 = 2732$) to confirm the above argument. For this purpose, we count the number of nodes $\tilde{\nu}_i(l)$ within distance l from every node i in the (2,2)-flower and calculate the local fractal dimension $d_f(i)$ according to the relation $\tilde{\nu}_i(l) \propto l^{d_f(i)}$ [31]. Figure 5(a) indicates the value of $d_f(i)$ at each node i by color. As expected, local fractal dimensions $d_f(i)$ take values close to $d_f^{min} = 1$ on high-degree nodes and close to $d_f^{max} = 2$ on low-degree nodes away from the high-degree nodes. It is due to the finite-size

effect that $d_f(i)$'s on some nodes take intermediate values between d_f^{min} and d_f^{max}. Regions around these nodes do not actually have fractality described by the intermediate d_f, but the least-squares fit for $\tilde{\nu}_i(l)$ of the finite-size network merely evaluates the dimensional crossover from d_f^{max} to d_f^{min} as if having the intermediate dimension. The scale-free property is crucial for the distribution of the local fractal dimension. In a fractal network without the scale-free property, the local fractality around any node is described by the global fractal dimension, as shown by Fig. 5(b). In this figure, $d_f(i)$ on every node in the seventh generation Sierpinski gasket ($N_7 = 3282$) is indicated. The computed $d_f(i)$'s take values close to the global fractal dimension $D_f = \log 3/\log 2(= 1.585)$ regardless of the node, except for nodes near the three corners affected by the finite-size effect.

V. CONCLUSION

In this work we have studied the structural multifractality of extensive classes of fractal scale-free networks (FSFNs) and conjectured that any FSFN possesses a bifractal structure characterized by two local fractal dimensions. It has been reported in previous work [23] that if the number of nodes in each of boxes covering an FSFN minimally is proportional to the number of adjacent boxes, namely, Eq. (2) holds, the network is bifractal. Based on this proposition, we first showed that deterministic hierarchical FSFNs formed by the single-generator model exhibit the bifractal nature in their structures. This result was confirmed for several deterministic hierarchical FSFNs by comparing the mass exponents $\tau(q)$ predicted theoretically with those calculated numerically. Next, we examined stochastic hierarchical FSFNs which have hierarchical structures but are not deterministic. In order to construct such FSFNs, we proposed the multigenerator model in which every edge in the previous generation network is recursively replaced with one of multiple generators with a certain probability. Our analytical argument reveals that FSFNs formed by this model also have bifractal structures. The bifractal profile of $\tau(q)$ for these networks has been verified numerically by employing several combinations of multiple generators. Furthermore, we showed that nonhierarchical FSFNs exhibit bifractality, by investigating the giant component of a scale-free random network at the percolation critical point. By evaluating the conditional probability describing the long-range degree correlation of the giant component and by utilizing it to count the number of nodes in a box and the number of neighboring boxes, we verified Eq. (2). Finally, we demonstrated that the mass exponents for two real-world FSFNs are consistent with the bifractal profiles of $\tau(q)$ predicted by their degree exponents and global fractal dimensions. From these results, we conjecture that any FSFN is bifractal. Moreover, we studied which substructures of an FSFN are characterized by its local fractal dimensions d_f^{min} and d_f^{max}. Our arguments clarified that d_f^{min} describes substructures around infinitely high-degree hub nodes and finite-degree nodes at finite distances from these hub nodes, while d_f^{max} describes the local fractality around finite-degree nodes infinitely far from infinite-degree hub nodes.

The bifractality in the strict sense is realized only in infinitely large FSFNs. However, even in a finite-size FSFN,

the fractality cannot be described only by the global fractal dimension D_f. Local structures near high-degree hub nodes are characterized by $d_f^{\min}$, and the fractality near low-degree nodes far from hub nodes is quantified by $d_f^{\max}$. Meanwhile, we expect a dimensional crossover in the vicinity of a low-degree node not far from the hub or a node with an intermediate degree. Therefore, the multifractal analysis for a finite-size FSFN makes it appear as if the network possesses multifractality described by an infinite number of local fractal dimensions, but this is merely a finite-size effect of the bifractal nature.

It is important to study how the structural bifractality affects phenomena occurring on FSFNs. Random walks on FSFNs, for example, can be influenced by bifractality of the networks. In fact, it has been reported that there are two distinct values of the spectral dimension d_s characterizing the time dependence of the return-to-origin probability of a random walker [34–36], though the distance dependence of the first-passage time is described only by a single walk dimension d_w [11]. Future research should clarify the relevance of these two spectral dimensions and the bifractal nature of the network, which will lead to a systematic understanding of various dynamics on bifractal networks.

APPENDIX A: DERIVATION OF EQ. (3)

Here we derive the bifractal mass exponent $\tau(q)$, namely Eq. (3), under the assumption Eq. (2). Given an FSFN $\mathcal{G}$ of N nodes, let us cover $\mathcal{G}$ with the minimum number $N_B(l)$ of boxes of diameter l, and assume that Eq. (2) holds for each box b. Equation (2) gives the relation

$$\nu_b = \frac{\langle \nu_b \rangle}{\langle k_b \rangle} k_b, \tag{A1}$$

where $\langle \nu_b \rangle$ and $\langle k_b \rangle$ are the mean values of ν_b and k_b averaged over the boxes, respectively. Since $\langle \nu_b \rangle = N/N_B(l)$, we have $\nu_b = k_b N / \langle k_b \rangle N_B(l)$ and the box measure $\mu_b = \nu_b/N$ is given by

$$\mu_b = \frac{k_b}{\langle k_b \rangle N_B(l)}. \tag{A2}$$

The number of boxes $N_B(l)$ is proportional to l^{-D_f}. Then the box measure μ_b is written as

$$\mu_b(k_b) \propto \frac{k_b}{\langle k_b \rangle} l^{D_f}. \tag{A3}$$

Therefore, the qth moment $Z_q(l)$ defined by Eq. (1) is calculated as

$$Z_q(l) = \sum_b \mu_b^q(k_b) \simeq N_B(l) \int_0^\infty \mu_b^q(k_b) P(k_b) \, dk_b$$

$$\propto \frac{l^{(q-1)D_f}}{\langle k \rangle^q} \int_0^\infty k^q P(k) \, dk, \tag{A4}$$

where $P(k_b)$ is the degree distribution of the supernode b in the renormalized network of $\mathcal{G}$, which is the same as the degree distribution $P(k) \propto k^{-\gamma}$ of the original network $\mathcal{G}$ due to the fractal property of $\mathcal{G}$.

In the case of $q - \gamma < -1$, the integral in Eq. (A4), namely, the qth moment of k, converges to a constant value. Thus, we have $Z_q(l) \propto l^{(q-1)D_f}$, which implies that $\tau(q) = (q-1)D_f$ for $q < \gamma - 1$. For $q \geqslant \gamma - 1$, however, the integral in Eq. (A4) must be evaluated by considering that $N_B(l)$ is sufficiently large but finite. In this case, the degree of the renormalized network is bounded by the natural cutoff $k_c(l) \propto [N_B(l)]^{1/(\gamma-1)} \propto l^{-D_f/(\gamma-1)}$ [47]. Hence, the qth moment becomes

$$Z_q(l) \propto \frac{l^{(q-1)D_f}}{\langle k \rangle^q} \int^{k_c(l)} k^{q-\gamma} \, dk$$

$$\propto l^{D_f q(\gamma-2)/(\gamma-1)}. \tag{A5}$$

This gives $\tau(q) = qD_f(\gamma-2)/(\gamma-1)$ for $q \geqslant \gamma - 1$.

APPENDIX B: PROPERTIES OF NETWORKS FORMED BY THE MULTIGENERATOR MODEL

Let us consider properties of the tth generation network $\mathcal{G}_t$ formed by the multigenerator model. If $\mathcal{G}_{t-1}$ contains M_{t-1} edges, $p^{(i)}M_{t-1}$ edges, on average, in $\mathcal{G}_{t-1}$ are replaced with $G_{\text{gen}}^{(i)}$ in the growth process from $\mathcal{G}_{t-1}$ to $\mathcal{G}_t$, and these edges proliferate to $p^{(i)}M_{t-1}m_{\text{gen}}^{(i)}$ in $\mathcal{G}_t$, where $m_{\text{gen}}^{(i)}$ is the number of edges in $G_{\text{gen}}^{(i)}$. Thus, the number of edges in $\mathcal{G}_t$ is given by $M_t = M_{t-1}\langle m_{\text{gen}} \rangle$, where $\langle m_{\text{gen}} \rangle = \sum_i^s m_{\text{gen}}^{(i)} p^{(i)}$ is the mean number of edges averaged over the multiple generators. Solving this recurrence equation under the condition $M_0 = 1$, the number of edges in $\mathcal{G}_t$ is given by

$$M_t = \langle m_{\text{gen}} \rangle^t. \tag{B1}$$

Regarding the number of nodes, $p^{(i)}M_{t-1}n_{\text{rem}}^{(i)}$ nodes in $\mathcal{G}_t$ emerge from $p^{(i)}M_{t-1}$ edges in $\mathcal{G}_{t-1}$ by the edge replacement operation with $G_{\text{gen}}^{(i)}$, where $n_{\text{rem}}^{(i)}$ is the number of remaining nodes of $G_{\text{gen}}^{(i)}$. The total number of newly emerged nodes in $\mathcal{G}_t$ is then given by $M_{t-1}\langle n_{\text{rem}} \rangle$, where $\langle n_{\text{rem}} \rangle = \sum_i^s n_{\text{rem}}^{(i)} p^{(i)}$ is the mean number of remaining nodes averaged over the multiple generators. Thus, using Eq. (B1), the number of nodes N_t in $\mathcal{G}_t$ is written as

$$N_t = N_{t-1} + \langle n_{\text{rem}} \rangle \langle m_{\text{gen}} \rangle^{t-1}. \tag{B2}$$

The solution of this recurrence equation under the initial condition $N_0 = 2$ is given as

$$N_t = 2 + \frac{\langle n_{\text{rem}} \rangle (\langle m_{\text{gen}} \rangle^t - 1)}{\langle m_{\text{gen}} \rangle - 1}. \tag{B3}$$

This expression is the same as Eq. (5) if we replace $\langle n_{\text{rem}} \rangle$ and $\langle m_{\text{gen}} \rangle$ by n_{rem} and m_{gen}, respectively. Since N_t is proportional

to $\langle m_{\mathrm{gen}}\rangle^t$ for $t \gg 1$ as can be seen from Eq. (B3), we have

$$N_t = \langle m_{\mathrm{gen}}\rangle N_{t-1}, \tag{B4}$$

for high-generation networks.

Next, we consider the asymptotic form of the degree distribution $P(k)$ for sufficiently large k and $t \gg 1$. Since $p^{(i)}k$ edges out of the k edges incident to a node of degree k are replaced with $G_{\mathrm{gen}}^{(i)}$, these $p^{(i)}k$ edges increase the degree of the node by $\kappa^{(i)}p^{(i)}k$ in the next generation, where $\kappa^{(i)}$ is the degree of the root node in $G_{\mathrm{gen}}^{(i)}$. Therefore, the number of nodes, $N_{t-1}(k)$, of degree k in $\mathcal{G}_{t-1}$ is the same as that of nodes of degree $\sum_i \kappa^{(i)}p^{(i)}k$ in $\mathcal{G}_t$, namely, $N_{t-1}(k) = N_t(\langle \kappa \rangle k)$, where $\langle \kappa \rangle = \sum_i \kappa^{(i)}p^{(i)}$ is the mean degree of the root nodes averaged over the generators. Using the asymptotic degree distribution $P(k)$ for $t \gg 1$, this relation can be written as $N_{t-1}P(k) = \langle \kappa \rangle N_t P(\langle \kappa \rangle k)$, and it follows from Eq. (B4) that

$$P(k) = \langle m_{\mathrm{gen}}\rangle\langle \kappa \rangle P(\langle \kappa \rangle k). \tag{B5}$$

The solution of this functional equation is $P(k) \propto k^{-\gamma}$ with

$$\gamma = 1 + \frac{\log\langle m_{\mathrm{gen}}\rangle}{\log\langle \kappa \rangle}. \tag{B6}$$

Thus, networks formed by this stochastic model possess the scale-free property.

We can also show that $\mathcal{G}_t$ with $t \gg 1$ has a fractal structure. In order to examine the fractal property of $\mathcal{G}_t$, we consider the distance l_t between two specific nodes in the network $\mathcal{G}_t$. Considering that edge replacements are performed randomly, we can expect a relation of $l_t = \langle \lambda \rangle l_{t-1}$ with some coefficient $\langle \lambda \rangle$ for $t \gg 1$, where l_{t-1} is the distance between the same node pair in $\mathcal{G}_{t-1}$. It should be emphasized that the mean inter-root-node distance $\langle \lambda \rangle$ is not given by the simple average $\sum_i \lambda^{(i)}p^{(i)}$, where $\lambda^{(i)}$ is the distance between root nodes in the generator $G_{\mathrm{gen}}^{(i)}$, because the shortest path itself may change due to the edge replacements. The correct $\langle \lambda \rangle$ can be calculated using the concept of renormalization. Since $\langle \lambda \rangle$ is independent of the choice of node pairs, let l_t be the distance between two nodes in $\mathcal{G}_t$ corresponding to the two terminal nodes of the zeroth-generation graph consisting of two nodes and a single edge. From a renormalization perspective, $\mathcal{G}_t$ takes a structure in which each edge of the generators is replaced with one of the possible structures from $\mathcal{G}_{t-1}$ with equal probability. Therefore, we have

$$l_t = \sum_{i=1}^{s} p^{(i)}l_t^{(i)}, \tag{B7}$$

with

$$l_t^{(i)} = F^{(i)}\big(\{l_{t-1}^{(j)}\}, \{p^{(j)}\}\big). \tag{B8}$$

Here $l_t^{(i)}$ is the average distance between root nodes in the generator $G_{\mathrm{gen}}^{(i)}$ in which each edge has one of the lengths $\{l_{t-1}^{(j)} : 1 \leqslant j \leqslant s\}$ with probability $p^{(j)}$, and $F^{(i)}$ is the function mapping from $\{l_{t-1}^{(j)}\}$ to $l_t^{(i)}$. Given the structures of the generators, the functional forms of $\{F^{(i)}\}$ are determined, and we can iteratively compute $l_t^{(i)}$ by Eq. (B8) and then obtain

l_t from Eq. (B7). From the relation $l_t = \langle \lambda \rangle l_{t-1}$, the mean inter-root-node distance $\langle \lambda \rangle$ is given by

$$\langle \lambda \rangle = \lim_{t \to \infty} \frac{l_t}{l_{t-1}}. \tag{B9}$$

Recalling that $\langle \lambda \rangle$ does not depend on the choice of node pairs, for the diameter L_t of the network $\mathcal{G}_t$ we have

$$L_t = \langle \lambda \rangle L_{t-1} \tag{B10}$$

for $t \gg 1$. Although the two nodes determining the diameter of $\mathcal{G}_t$ may be slightly distant from the nodes giving the diameter of $\mathcal{G}_{t-1}$, Eq. (B10) is valid for sufficiently large t. The combination of Eqs. (B4) and (B10) implies that as the network diameter becomes $\langle \lambda \rangle$ times larger, the number of nodes increases by a factor of $\langle m_{\mathrm{gen}}\rangle$. This leads to the relation $N_t \propto L_t^{D_\mathrm{f}}$ with

$$D_\mathrm{f} = \frac{\log\langle m_{\mathrm{gen}}\rangle}{\log\langle \lambda \rangle}. \tag{B11}$$

As an example, let us calculate D_f for the combination of the black generators shown in Fig. 3. Setting $G_{\mathrm{gen}}^{(1)}$ and $G_{\mathrm{gen}}^{(2)}$ as the generators with four and six nodes, respectively, the functions $F^{(1)}$ and $F^{(1)}$ are given by

$$
\begin{aligned}
&F^{(1)}\big(l_t^{(1)}, l_t^{(2)}, p\big) \\
&= 2l_t^{(1)}p^4 + 4\min\big(l_t^{(1)} + l_t^{(2)}, 2l_t^{(1)}\big)p^3(1-p) \\
&\quad + 2\min\big(2l_t^{(1)}, 2l_t^{(2)}\big)p^2(1-p)^2 + 4\big(l_t^{(1)} + l_t^{(2)}\big)p^2(1-p)^2 \\
&\quad + 4\min\big(l_t^{(1)} + l_t^{(2)}, 2l_t^{(2)}\big)p(1-p)^3 + 2l_t^{(2)}(1-p)^4,
\end{aligned}
\tag{B12}
$$

$$
\begin{aligned}
&F^{(2)}\big(l_t^{(1)}, l_t^{(2)}, p\big) \\
&= 3l_t^{(1)}p^5 + 2 \cdot 3l_t^{(1)}p^4(1-p) + 3\big(2l_t^{(1)} + l_t^{(2)}\big)p^4(1-p) \\
&\quad + 6\big(2l_t^{(1)} + l_t^{(2)}\big)p^3(1-p)^2 + 3l_t^{(1)}p^3(1-p)^2 \\
&\quad + 3\big(l_t^{(1)} + 2l_t^{(2)}\big)p^3(1-p)^2 + 3l_t^{(2)}p^2(1-p)^3 \\
&\quad + 6\big(l_t^{(1)} + 2l_t^{(2)}\big)p^2(1-p)^3 + 3\big(2l_t^{(1)} + l_t^{(2)}\big)p^2(1-p)^3 \\
&\quad + 2 \times 3l_t^{(2)}p(1-p)^4 + 3\big(l_t^{(1)} + 2l_t^{(2)}\big)p(1-p)^4 \\
&\quad + 3l_t^{(2)}(1-p)^5,
\end{aligned}
\tag{B13}
$$

where p is the edge replacement probability for $G_{\mathrm{gen}}^{(1)}$, and the function $\min(x, y)$ returns the minimum value of x and y. These functions $F^{(1)}$ and $F^{(2)}$ enable us to calculate the mean distance $\langle \lambda \rangle$ from Eqs. (B7)–(B9). For $p = 1/2$ as in the case of Fig. 3, for example, $\langle \lambda \rangle$ given by Eq. (B9) rapidly converges to $\langle \lambda \rangle = 2.408$. Since $\langle m_{\mathrm{gen}}\rangle = 9/2$ for these $G_{\mathrm{gen}}^{(1)}$ and $G_{\mathrm{gen}}^{(2)}$, the fractal dimension for $p = 1/2$ is $D_\mathrm{f} = 1.712$. This value, of course, varies with p from $D_\mathrm{f} = \log 5/\log 2 = 1.465$ ($p = 0$) to $D_\mathrm{f} = 2$ ($p = 1$), which implies that we can continuously control the fractality of FSFNs by using the multigenerator model.

The above results show that networks built by the multigenerator model are FSFNs as in the case of the single-generator model. We should note that the expressions of M_t, N_t, γ, and D_f are the same as those for the single-generator model if we replace quantities characterizing the single generator by their mean values for the multiple generators.

[1] A.-L. Barabási and R. Albert, Science **286**, 509 (1999).

[2] R. Albert and A.-L. Barabási, Rev. Mod. Phys. **74**, 47 (2002).

[3] M. E. J. Newman, SIAM Rev. **45**, 167 (2003).

[4] M. E. J. Newman, S. H. Strogatz, and D. J. Watts, Phys. Rev. E **64**, 026118 (2001).

[5] C. Song, S. Havlin, and H. A. Makse, Nature (London) **433**, 392 (2005).

[6] C. Song, S. Havlin, and H. A. Makse, Nat. Phys. **2**, 275 (2006).

[7] K.-I. Goh, G. Salvi, B. Kahng, and D. Kim, Phys. Rev. Lett. **96**, 018701 (2006).

[8] C. Song, L. K. Gallos, S. Havlin, and H. A. Makse, J. Stat. Mech. (2007) P03006.

[9] L. K. Gallos, C. Song, and H. A. Makse, Physica A **386**, 686 (2007).

[10] J. S. Kim, K.-I. Goh, G. Salvi, E. Oh, B. Kahng, and D. Kim, Phys. Rev. E **75**, 016110 (2007).

[11] H. D. Rozenfeld, S. Havlin, and D. ben-Avraham, New J. Phys. **9**, 175 (2007).

[12] H. D. Rozenfeld, C. Song, and H. A. Makse, Phys. Rev. Lett. **104**, 025701 (2010).

[13] A. Watanabe, S. Mizutaka, and K. Yakubo, J. Phys. Soc. Jpn. **84**, 114003 (2015).

[14] Y. Fujiki and K. Yakubo, Phys. Rev. E **101**, 032308 (2020).

[15] Y. Fujiki, S. Mizutaka, and K. Yakubo, Eur. Phys. J. B **90**, 126 (2017).

[16] E. Rosenberg, *Fractal Dimensions of Networks* (Springer International Publishing, Cham, 2020).

[17] G. Concas, M. F. Locci, M. Marchesi, S. Pinna, and I. Turnu, Europhys. Lett. **76**, 1221 (2006).

[18] Y. Zhang, Z. Zhang, and J. Guan, J. Phys. A: Math. Theor. **40**, 12365 (2007).

[19] M. Kitsak, S. Havlin, G. Paul, M. Riccaboni, F. Pammolli, and H. E. Stanley, Phys. Rev. E **75**, 056115 (2007).

[20] W.-X. Zhou, Z.-Q. Jiang, and D. Sornette, Physica A **375**, 741 (2007).

[21] M. Guida and F. Maria, Chaos, Solitons & Fractals **31**, 527 (2007).

[22] F. Kawasaki and K. Yakubo, Phys. Rev. E **82**, 036113 (2010).

[23] S. Furuya and K. Yakubo, Phys. Rev. E **84**, 036118 (2011).

[24] B. B. Mandelbrot, J. Fluid Mech. **62**, 331 (1974).

[25] D.-L. Wang, Z.-G. Yu, and V. Anh, Chinese Phys. B **21**, 080504 (2012).

[26] B.-G. Li, Z.-G. Yu, and Y. Zhou, J. Stat. Mech. (2014) P02020.

[27] J.-L. Liu, Z.-G. Yu, and V. Anh, Chaos **25**, 023103 (2015).

[28] S. Rendón de la Torre, J. Kalda, R. Kitt, and J. Engelbrecht, Eur. Phys. J. B **90**, 234 (2017).

[29] E. Rosenberg, Phys. Lett. A **381**, 2222 (2017).

[30] P. Pavón-Domínguez and S. Moreno-Pulido, Physica A **541**, 123670 (2020).

[31] X. Xiao, H. Chen, and P. Bogdan, Sci. Rep. **11**, 22964 (2021).

[32] Y. Ding, J.-L. Liu, X. Li, Y-C. Tian, and Z-G. Yu, Phys. Rev. E **103**, 043303 (2021).

[33] P. Pavón-Domínguez and S. Moreno-Pulido, Chaos, Solitons & Fractals **156**, 111836 (2022).

[34] S. Hwang, D.-S. Lee, and B. Kahng, Phys. Rev. E **85**, 046110 (2012).

[35] S. Hwang, D.-S. Lee, and B. Kahng, Phys. Rev. Lett. **109**, 088701 (2012).

[36] S. Hwang, D.-S. Lee, and B. Kahng, Phys. Rev. E **87**, 022816 (2013).

[37] K. Yakubo and Y. Fujiki, PLoS ONE **17**, e0264589 (2022).

[38] P. Bialas and A. K. Oleś, Phys. Rev. E **77**, 036124 (2008).

[39] R. Cohen, S. Havlin, and D. ben-Avraham, in *Handbook of Graphs and Networks*, edited by S. Bornholdt and H. G. Schuster (Wiley-VCH, New York, 2003), pp. 85–110.

[40] Y. Fujiki, T. Takaguchi, and K. Yakubo, Phys. Rev. E **97**, 062308 (2018).

[41] S. Mizutaka and T. Hasegawa, J. Phys. Complex. **1**, 035007 (2020).

[42] M. Molloy and B. Reed, Random Struct. Alg. **6**, 161 (1995).

[43] E. A. Bender and E. R. Canfield, J. Comb. Theory, Ser. A **24**, 296 (1978).

[44] R. Albert, H. Jeong, and A.-L. Barabási, Nature (London) **401**, 130 (1999).

[45] R. M. Ewing, P. Chu, F. Elisma, H. Li, P. Taylor, S. Climie, L. McBroom-Cerajewski, M. D. Robinson, L. O'Connor, M. Li *et al.*, Mol. Syst. Biol. **3**, 89 (2007).

[46] T. P. Peixoto, The Netzschleuder Network Catalogue and Repository, https://networks.skewed.de.

[47] S. N. Dorogovtsev and J. F. F. Mendes, Adv. Phys. **51**, 1079 (2002).